CrossMark

The impact of injector-based contrast agent administration in time-resolved MRA

Johannes Budjan[1] · Ulrike I. Attenberger[1] · Stefan O. Schoenberg[1] · Hubertus Pietsch[2] ·
Gregor Jost[2]

Abstract

Objectives Time-resolved contrast-enhanced MR angiography (4D-MRA), which allows the simultaneous visualization of the vasculature and blood-flow dynamics, is widely used in clinical routine. In this study, the impact of two different contrast agent injection methods on 4D-MRA was examined in a controlled, standardized setting in an animal model.

Methods Six anesthetized Goettingen minipigs underwent two identical 4D-MRA examinations at 1.5 T in a single session. The contrast agent (0.1 mmol/kg body weight gadobutrol, followed by 20 ml saline) was injected using either manual injection or an automated injection system. A quantitative comparison of vascular signal enhancement and quantitative renal perfusion analyses were performed.

Results Analysis of signal enhancement revealed higher peak enhancements and shorter time to peak intervals for the automated injection. Significantly different bolus shapes were found: automated injection resulted in a compact first-pass bolus shape clearly separated from the recirculation while manual injection resulted in a disrupted first-pass bolus with two peaks. In the quantitative perfusion analyses, statistically significant differences in plasma flow values were found between the injection methods.

Conclusions The results of both qualitative and quantitative 4D-MRA depend on the contrast agent injection method, with automated injection providing more defined bolus shapes and more standardized examination protocols.

Key points
• *Automated and manual contrast agent injection result in different bolus shapes in 4D-MRA.*
• *Manual injection results in an undefined and interrupted bolus with two peaks.*
• *Automated injection provides more defined bolus shapes.*
• *Automated injection can lead to more standardized examination protocols.*

Keywords Magnetic resonance angiography ·
Magnetic resonance imaging · Contrast media ·
Perfusion MRI · Contrast-enhanced MRI

✉ Johannes Budjan
johannes.budjan@umm.de

1 Department of Clinical Radiology and Nuclear Medicine, University Medical Center Mannheim, Medical Faculty Mannheim – Heidelberg University, Theodor-Kutzer-Ufer 1-3, 68167 Mannheim, Germany

2 MR and CT Contrast Media Research, Bayer AG, Berlin, Germany

Introduction

With the introduction and refinement of view-sharing and keyhole magnetic resonance (MR) imaging techniques, time-resolved contrast-enhanced (CE) MR angiography (4D-MRA) sequences that provide both high temporal and high spatial resolution have become available for use in clinical routine. Today, 4D-MRA sequences that can cover large imaging volumes and visualize the passage of a vascular contrast agent (CA) over time are available on almost all MR scanner systems. There are numerous applications for 4D-MRA, which are related to either vessel pathologies [1] (including vascular tumors) or (quantitative) perfusion assessment [2]. In comparison to conventional static 3D-MRA, timing of the acquisition to obtain maximum arterial enhancement without venous overlay is far less critical in 4D-MRA [3, 4]. Optimal arterial phases can be selected retrospectively and

independently for different vessel regions, which can improve the diagnostic performance of MRA studies [5]. The additional information regarding flow dynamics has been shown to improve diagnostic performance and influence therapeutic decision-making in the context of aortic dissection [6], and in both diagnosis and therapy planning in vascular malformations [7] and carotid–cavernous fistulas [8].

Besides the direct visualization of hemodynamics in vessel-related pathologies, 4D-MRA can be used to calculate tissue blood flow and other quantitative perfusion parameters. Different algorithms, of which model-free deconvolution methods are the most general approaches [9, 10], can be applied to 4D-MRA datasets to obtain quantitative perfusion values. Quantitative or semiquantitative information about organ perfusion is of great interest in evaluation of renal [11, 12] and hepatic [13–15] pathologies, as well as in the assessment of tumor aggressiveness [16] and therapy response [14, 17, 18], and in the detection of tumor recurrence [19].

CE 4D-MRA is based on the intravenous administration of a gadolinium-based CA, which can be injected either manually or by a fully automated injection system. It is reasonable to assume that quantitative 4D-MRA in particular should be performed using automated injection. Besides a recent study assessing the impact of injection method on static MRA [20], there is no demonstrated or documented 'substantial knowledge' on this topic. However, most of those working in the field consider intuitively that automated injection can ensure a standardized and well-controlled injection. Nevertheless, hand injections are still frequently used for MRA procedures. A recent German survey revealed that only 62.1% of all MRA procedures were performed with automated injection [21], and in the USA, injector systems were found to be used in 72.7% of MRA examinations [22]. Additionally, manual injection is widely used in pediatric imaging, for both conventional and quantitative MRI [23–25]. Previous literature favors the use of automated injector systems for both MRA [26] and perfusion imaging applications [27]. However, to our knowledge, there are no published data showing the effects of different injection methods on either signal intensity changes over time in the vascular system or quantitative perfusion values in an in-vivo intraindividual comparison. The aim of this study was to compare fully automated CA administration with manual injection in 4D-MRA under highly standardized conditions in an animal model.

Materials and methods

Animals

Six Goettingen minipigs were examined. The animals were handled in compliance with German animal welfare legislation and with the approval of the state animal welfare committee. All studies were performed under general anesthesia induced by intramuscular injection of ketamine (30 mg/kg body weight; Pharmacia, Karlsruhe, Germany), azaperone (2 mg/kg; Stresnil, Janssen-Cilag, Neuss, Germany) and atropine (0.025 mg/kg; Eifelfango Chem.-Pharm. Werke, Bad Neuenahr-Ahrweiler, Germany). After intravenous administration of 1.4 mg/kg propofol (Propofol-Lipuro; B. Braun, Melsungen, Germany) and 1 µg/kg fentanyl (Janssen-Cilag GmbH, Neuss, Germany), the animals were orally intubated and mechanically ventilated with an oxygen/air mixture. Anesthesia was maintained by intravenous injection of propofol (0.8 mg/kg/h) and fentanyl (1 µg/kgh). Animals were placed in a prone position and MRA was performed during end-expiratory breath-hold. The heart rate was recorded before each CA administration.

MRA technique

MRI was performed with a clinical 1.5-T MR scanner (Avanto, Siemens Healthcare GmbH, Erlangen, Germany) using a spine coil in combination with a body matrix coil. For the 4D-MRA of the thoracic–abdominal region, a time-resolved angiography with interleaved stochastic trajectories (TWIST) sequence was used. Sequence parameters were: TR/TE/flip angle 2.41 ms/0.87 ms/25°, PAT factor 2 (GRAPPA), TWIST sampling rate A/B 20%/25%, voxel size 1.7 × 1.7 × 1.7 mm, 25 stacks with a 2-s image update time (55 s measurement time).

Contrast agent injection protocols

Gadobutrol (Gadovist; Bayer Vital GmbH, Leverkusen, Germany) was administered at a dosage of 0.1 mmol/kg body weight intravenously via an ear vein using a 20-gauge access. The CA injections were followed by a 20-ml saline chaser. To obtain intraindividual comparisons, each animal received the two CA injections (automated and manual) in a randomized order with a resting time for CA wash-out of at least 60 min between consecutive injections. For manual CA administration, a saline-prefilled patient tubing set (ProSet, Braun) was used in combination with a 5-ml syringe (Omnifix, Braun) that contained the body weight-adapted volume of CA. Immediately after CA injection, the syringes were changed and 20 ml saline was administered (Omnifix, 20-ml syringe). All manual administrations were done by the same experienced technician, who had performed more than 1,000 hand injections, and was instructed to administer the injection at a flow rate of approximately 2 ml/s. Automated injection was performed with a dual-head injection system (MRXperion; Bayer, Indianola, PA, USA) and a selected flow rate of 2 ml/s for CA and saline.

Quantitative analysis of signal enhancement

Quantitative analysis of the signal enhancement over time (bolus curves) was performed by one experienced reader (28 years experience in preclinical MRI), blinded to the experimental groups on the subtraction images using Mean Curve software on an external workstation (MMWP; Siemens Healthcare). Regions of interest (ROIs) were placed in the ascending aorta, the descending aorta (level of the truncus pulmonalis), the abdominal aorta (level of the truncus coeliacus and below the kidneys), the renal arteries and the inferior vena cava (above the kidneys). The first-pass bolus peak signal intensity (PSI) and the time to peak (TTP) interval were determined for each region.

Quantitative perfusion analysis

For the quantitative perfusion analysis, three different perfusion maps, including plasma flow (PF), mean transit time (MTT) and volume of distribution (VoD), were calculated using the fast deconvolution approach of the UMMPerfusion tool (version 1.5.3, running on OsiriX version 5.6; OsiriX Foundation, Geneva, Switzerland) [28, 29]. This tool uses a modified version of the model-free deconvolution algorithm originally proposed by Ostergaard et al. [29, 30]. A linear relationship between CA concentration and signal intensity is assumed. The unknown tissue-specific impulse response function can be derived by numerical deconvolution from the measured signal intensity–time curves of the tissue and the feeding artery (arterial input function, AIF) without making any additional assumptions concerning the interior structure of the tissue [31]. The impulse response function can then be used to obtain additional parameters such as MTT and VoD. For all calculations, hematocrit was set to 0.45. To generate the AIF, a ROI was placed in the abdominal aorta at the level of the renal arteries. Quantitative values were obtained as mean values over the entire manually segmented kidney volumes. Placement of AIF ROIs and kidney segmentation was performed by a single radiologist with 4 years experience in abdominal MRI.

Statistical evaluation

All values are given as means ± standard deviation. For the analysis of PSI and TTP, a two-way repeated-measures analysis of variance (ANOVA) with vessel and injection method as variables was used. The repeated t test was used for statistical comparison of heart rates. A paired t test was used for comparison of renal perfusion values. The calculations were performed with GraphPad Prism (GraphPad Software, La Jolla, CA, USA) using a significance level of 5%.

Results

The MR examination protocol including both 4D-MRA sequences with (1) manual and (2) injector-based CA administration was performed successfully in all six animals (one male animal, 40.6 ± 1.0 kg). Representative MRA images for different time points for both injection methods are shown in Fig. 1. The animals' average heart rate did not differ between the manual and the automated injection 4D-MRA sequence acquisitions (107.2 ± 7.7 bpm vs. 109.7 ± 9.2 bpm, $p = 0.63$).

Quantitative analysis of signal enhancement

The time-resolved analysis of the signal enhancement representing the bolus curve revealed higher PSI in all assessed anatomical regions for the automated injection compared with manual injection (the mean PSI values are shown in Table 1). In the statistical analysis, PSI differed significantly between the injection methods ($p < 0.0001$), among vessel regions ($p < 0.003$) and among subjects ($p = 0.003$). TTP was lower for the automated injection method in all vessel regions (Table 1). Likewise, TTP differed significantly between the injection method ($p = 0.0114$) and among vessel regions ($p < 0.0001$), but not among subjects ($p = 0.27$).

Assessment of bolus shapes

Bolus shapes differed significantly between the two injection methods. Use of the fully automated injection system resulted in a compact first-pass bolus shape that was clearly separated from the second-pass bolus, the latter representing CA recirculation. With manual injection, the first-pass bolus was disrupted into two peaks, a dominating first peak, closely followed by a second peak with lower signal intensity (Fig. 2). This led to a prolonged first-pass bolus filling the gap (i.e. signal decline) seen between the first and second pass. This additional peak was seen in all vascular regions investigated. These differences between the two injection methods were consistently found in all six animals (Fig. 3).

Quantitative perfusion analysis

In the perfusion analysis, automated injection led to higher renal PF values (234.5 ± 63.4 ml/100 ml/min for automated injection vs. 187.8 ± 34.1 ml/100 ml/min for manual injection, Fig. 4) and lower MTT (9.1 ± 1.4 s for automated injection vs. 10.2 ± 0.9 s for manual injection), while VoD was the same for both injection protocols (29.9 ± 6.9 ml/100 ml for automated injection vs. 29.3 ± 5.1 ml/100 ml for manual injection). PF and MTT showed statistically significant differences in the one-tailed paired analysis between the injection methods ($p = 0.0461$ and $p = 0.047$, respectively).

Fig. 1 Maximum intensity projections for different time-points (**a**, **d** pulmonary artery; **b**, **e** arterial phase; **c**, **f** venous phase) of the subtracted 4D-MRA datasets for manual injection (top row **a**–**c**) and automated injection (bottom row **d**–**f**). Note the differences in contrast enhancement in the aorta (arrows) during the venous phase due to the prolonged bolus of the manual injection
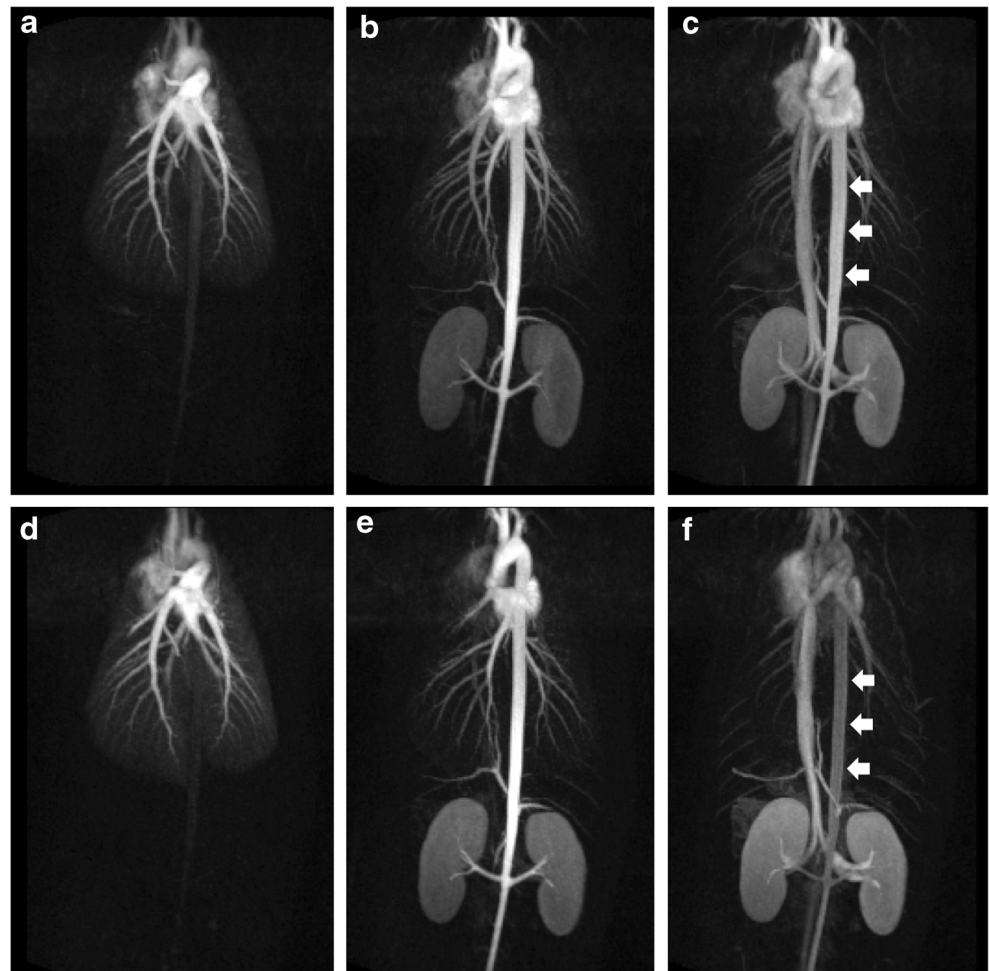

Discussion

In CE 4D-MRA, the flow of a CA through the vascular system is one of the central factors influencing vessel signal intensity. The flow of CA is influenced by patient-specific factors (such as cardiac output), by the vessel itself or vessel-related pathology (such as stenosis) and by the way the CA is injected [32–34]. As patient-specific and pathology-specific factors that influence CA flow are variable, standardization of the CA injection method seems to be a logical step to reduce variability and increase reproducibility of CE MRI techniques, in particular 4D-MRA. Well-defined bolus shapes seem to be important particularly for determining quantitative values and for comparing

Table 1 Peak signal intensities and times to peak for different vessel regions

| Vessel region	Peak signal intensity (a.u.)		Time to peak (s)	
	Manual injection	Automated injection	Manual injection	Automated injection
Ascending aorta	334.1 ± 62.5	372.4 ± 45.9	23.7 ± 2.9	22.4 ± 1.1
Descending aorta				
Truncus pulmonalis level	258.3 ± 57.9	291.8 ± 48.3	24.1 ± 3.0	23.4 ± 0.0
Truncus coeliacus level	333.7 ± 26.9	361.8 ± 39.1	25.4 ± 3.8	22.7 ± 1.0
Below the kidneys	270.3 ± 36.3	280.7 ± 63.4	26.1 ± 3.0	25.1 ± 1.0
Renal artery	194.5 ± 34.9	231.3 ± 53.9	26.4 ± 2.8	25.7 ± 1.5
Vena cava	185.6 ± 26.2	233.6 ± 30.1	35.0 ± 4.6	32.1 ± 2.0

a.u. arbitrary units
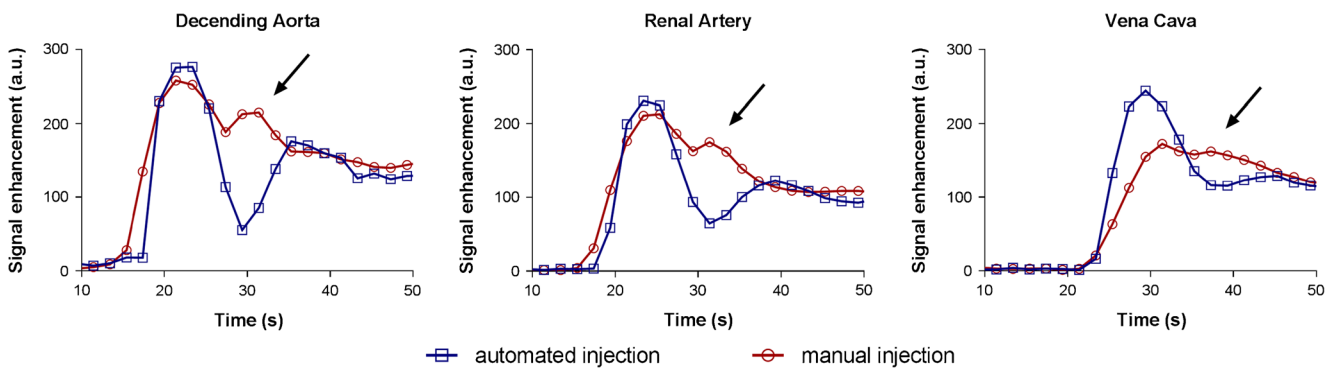
Fig. 2 Representative bolus curves from animal 3. An additional bolus peak (arrows) is found in all vascular regions when using hand injection (a.u. arbitrary units)

these values over different time points or between patients. Various studies evaluated the performance of perfusion MRI-derived values for the assessment of therapy response and found promising results for different entities (e.g. hepatic [35, 36] and head and neck [37] malignancies). In these applications, robust and reproducible techniques seem to be essential to allow valid longitudinal assessment.

Manual injection is operator-dependent and typically results in less precise injection rates. Even though a trained operator might be able to inject at a relatively constant rate during a specific examination, the variability in overall flow rates between different examinations (e.g. on different days) would likely be significant. The unavoidable short interruption during manual injection when switching the syringes from CA to saline had an even more significant effect on 4D-MRA bolus shapes than the potential variability in flow

rate in our study. After switching from CA to saline, the remaining CA in the injection line is pushed forwards by the saline, leading to disrupted CA flow. Even though this interruption was relatively short (typically in the range of 1–2 s), it led to an additional vascular peak in all examined vascular territories. The resulting undefined bolus profile might impair flow analysis and potentially distort the diagnostic information, e.g. in the evaluation of therapy response in vascular tumors treated by minimally invasive approaches (e.g. embolization or sclerotherapy [38]). In semiquantitative evaluation approaches, the degree of remaining vascularization and the decrease in vascularization of vascular malformations can probably be assessed more reliably using standardized injection protocols. Variability in bolus shapes might mimic therapy effects by indicating apparent differences in vascularity and flow dynamics of lesions.
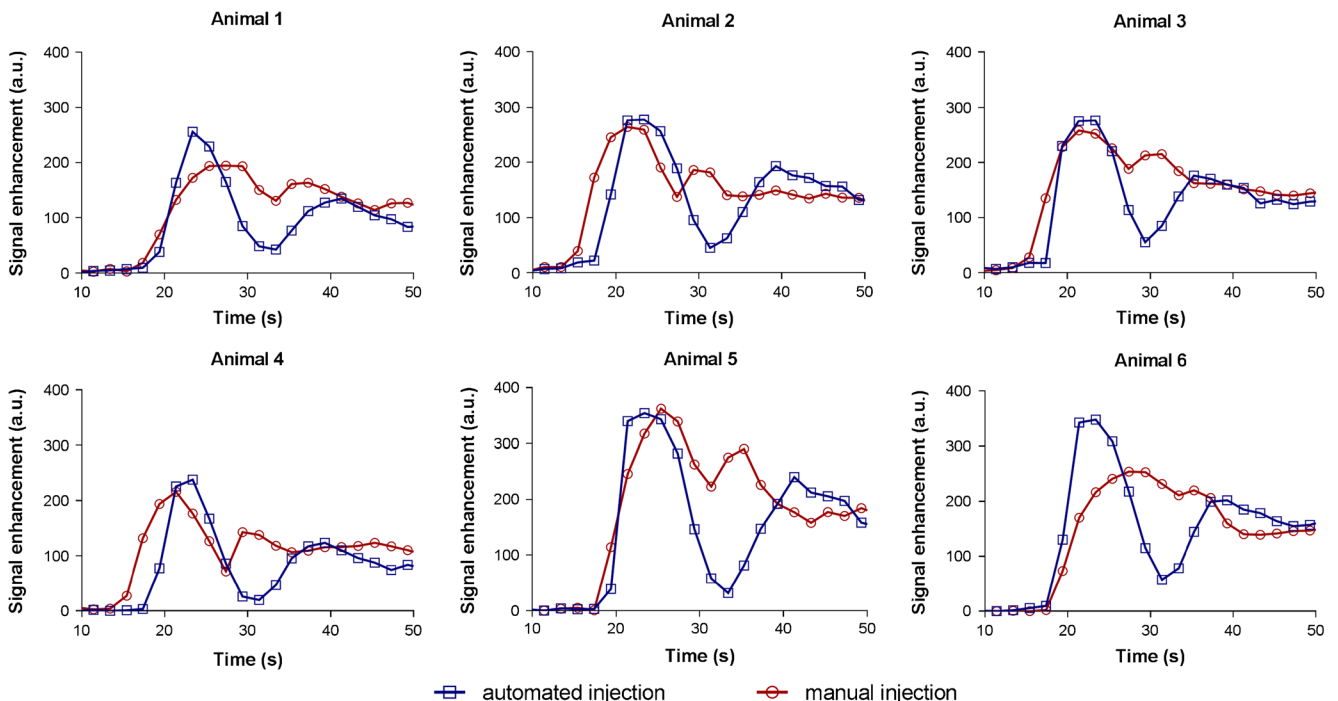
Fig. 3 Bolus curves at the level of the descending aorta for all 6 animals (a.u. arbitrary units)
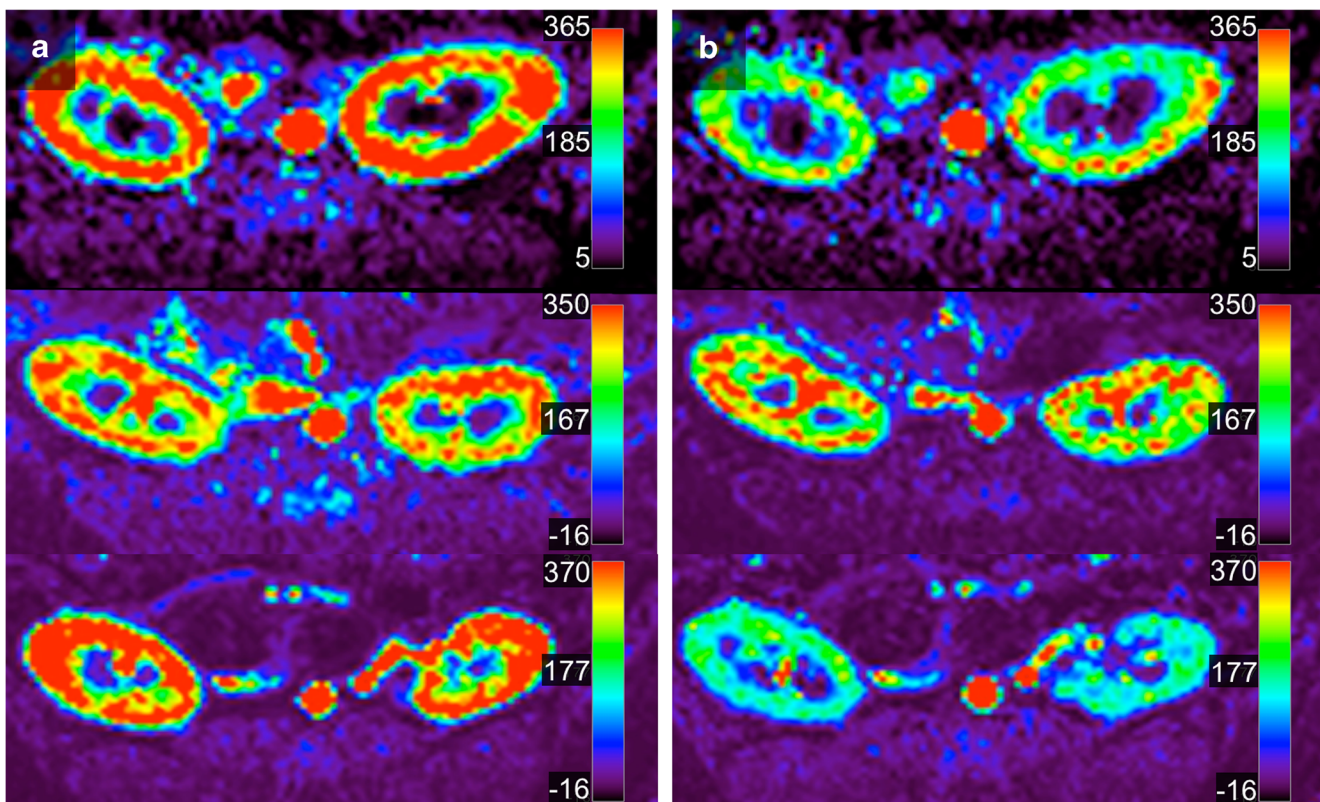
Fig. 4 Perfusion maps for three animals showing color-coded plasma flow for automated injection (**a**) and manual injection (**b**). Higher plasma flow values are apparent when using the automated injection protocol. Scale units are milliliters per 100 ml per minut

As the observed overlying second peak with manual injection protocols is influenced by recirculation time, the variability in the bolus curve shape is additionally influenced by patient-specific parameters. This might lead to further increased variability in bolus curve shapes. With the use of an automated injection system, injection of the saline chaser starts instantaneously, which yields continuous administration of the CA and thus a standardized vascular bolus shape. This may improve the reliability of information derived from the analysis of flow dynamics in 4D-MRA, as changes in flow characteristics e.g. in vessel territories or in vascular tumors after therapy can more likely be attributed to pathology or therapy-related effects rather than to variability in the technique itself [39–41]. To minimize the effect of bolus shapes on quantitative, absolute perfusion parameters, the model-free approach applied in this study used pixel-by-pixel deconvolution of the measured signal intensity–time curves in the tissue and the AIF. However, the highly disrupted bolus during manual injection led to distortion of the AIF, which was not equalized by the algorithm and resulted in different absolute perfusion values. This effect of manual in contrast to automated injection on quantitative results in model-free deconvolution approaches is of great interest and has, to our knowledge, not been shown in any previous studies in an in-vivo intraindividual comparison setup.

The additionally higher PSI and thus higher vessel to background contrast found with automated injection examinations might be of importance when assessing small vessels or smaller hypervascularized lesions. Although not evaluated explicitly in this study in healthy animals, an increased PSI and standardized TTP probably results in improved image quality, e.g. regarding vessel to background delineation [20, 42]. This may increase the diagnostic performance of dynamic MRA sequences, especially when combined with improved sequence and reconstruction techniques [43].

Limitations

The study was performed with a relatively low number of animals, which limits its statistical power. However, the differences in bolus shape between the two injection methods were found consistently in all animals (see Fig. 3). In this study, vascular signal enhancement instead of signal-to-noise was used for the quantitative comparison of MRA image quality. Noise measurements are challenging with the phased array coils used and with the use of parallel imaging reconstruction methods [44], and were not performed. However, intraindividual comparison in one imaging session allowed quantitative evaluation on the basis of signal intensity measurements [45].

In this study, all manual injections were performed by the same operator, who took special care to keep the flow rates and timings as close as possible. In clinical practice, manual injections will be performed by different operators, leading to even more heterogeneous bolus shapes. This is of special interest if 4D-MRA-derived quantitative perfusion values are measured over time, e.g. to evaluate therapy response. The short interruption in CA flow due to changing the syringe from contrast to saline during manual injection is unavoidable; the duration of the interruption is probably also operator-dependent. Thus, the use of the largely different shapes of AIF and parenchymal enhancement curves in the assessment of changes in perfusion will probably lead to distorted values that do not represent the true therapy-induced changes in perfusion.

As the absolute quantitative perfusion values were not the focus of this study, no reference standard measurement for renal perfusion was performed. However, the quantitative renal perfusion values found in this study are in good agreement with previously published values. Renal perfusion values for mean cortical perfusion in pigs have been found to lie in the range 180–235 ml/100 ml/min in previous studies based on Doppler ultrasonography, CT and MRI [46–48].

In conclusion, this animal study demonstrated that the use of a fully automated injection system enables the administration of CA and saline under highly reproducible conditions. This results in a clearly defined and standardized bolus shape and higher signal enhancement in 4D-MRA compared with manual injection. This might be especially relevant for vascular flow and quantitative perfusion analyses.

Compliance with ethical standards

Guarantor The scientific guarantor of this publication is Gregor Jost.

Conflict of interest G. Jost and H. Pietsch are employees of Bayer AG.

Statistics and biometry No complex statistical methods were necessary for this paper.

Ethical approval Approval from the institutional animal care committee was obtained.

Methodology
• prospective
• experimental
• performed at one institution

References

1. Morelli JN, Ai F, Runge VM et al (2012) Time-resolved MR angiography of renal artery stenosis in a swine model at 3 Tesla using gadobutrol with digital subtraction angiography correlation. J Magn Reson Imaging 36:704–713
2. Blackham KA, Passalacqua MA, Sandhu GS, Gilkeson RC, Griswold MA, Gulani V (2011) Applications of time-resolved MR angiography. AJR Am J Roentgenol 196:W613–W620
3. Schoenberg SO, Bock M, Knopp MV et al (1999) Renal arteries: optimization of three-dimensional gadolinium-enhanced MR angiography with bolus-timing-independent fast multiphase acquisition in a single breath hold. Radiology 211:667–679
4. Prince MR, Chabra SG, Watts R et al (2002) Contrast material travel times in patients undergoing peripheral MR angiography. Radiology 224:55–61
5. Voth M, Haneder S, Huck K, Gutfleisch A, Schonberg SO, Michaely HJ (2009) Peripheral magnetic resonance angiography with continuous table movement in combination with high spatial and temporal resolution time-resolved MRA with a total single dose (0.1 mmol/kg) of gadobutrol at 3.0 T. Invest Radiol 44:627–633
6. Kinner S, Eggebrecht H, Maderwald S et al (2015) Dynamic MR angiography in acute aortic dissection. J Magn Reson Imaging 42:505–514
7. Kramer U, Ernemann U, Mangold S et al (2012) Diagnostic value of high spatial and temporal resolution time-resolved MR angiography in the workup of peripheral high-flow vascular malformations at 1.5 Tesla. Int J Cardiovasc Imaging 28:823–834
8. Seeger A, Kramer U, Bischof F et al (2015) Feasibility of noninvasive diagnosis and treatment planning in a case series with carotid-cavernous fistula using high-resolution time-resolved MR-angiography with stochastic trajectories (TWIST) and extended parallel acquisition technique (ePAT 6) at 3 T. Clin Neuroradiol 25:241–247
9. Notohamiprodjo M, Reiser MF, Sourbron SP (2010) Diffusion and perfusion of the kidney. Eur J Radiol 76:337–347
10. Schaafs LA, Porter D, Audebert HJ, Fiebach JB, Villringer K (2016) Optimising MR perfusion imaging: comparison of different software-based approaches in acute ischaemic stroke. Eur Radiol 26:4204–4212
11. Sade R, Kantarci M, Karaca L et al (2017) Value of dynamic MRI using the Ktrans technique for assessment of native kidneys in pre-emptive renal transplantation. Acta Radiol 58:1005–1011
12. Notohamiprodjo M, Kalnins A, Andrassy M et al (2016) Multiparametric functional MRI: a tool to uncover subtle changes following allogeneic renal transplantation. PLoS One 11:e0165532
13. Thng CH, Koh TS, Collins D, Koh DM (2014) Perfusion imaging in liver MRI. Magn Reson Imaging Clin N Am 22:417–432
14. Ronot M, Clift AK, Vilgrain V, Frilling A (2016) Functional imaging in liver tumours. J Hepatol 65:1017–1030
15. Zhang W, Chen HJ, Wang ZJ, Huang W, Zhang LJ (2017) Dynamic contrast enhanced MR imaging for evaluation of angiogenesis of hepatocellular nodules in liver cirrhosis in N-nitrosodiethylamine induced rat model. Eur Radiol 27:2086–2094
16. Sanz-Requena R, Marti-Bonmati L, Perez-Martinez R, Garcia-Marti G (2016) Dynamic contrast-enhanced case-control analysis in 3T MRI of prostate cancer can help to characterize tumor aggressiveness. Eur J Radiol 85:2119–2126
17. Zheng D, Yue Q, Ren W et al (2016) Early responses assessment of neoadjuvant chemotherapy in nasopharyngeal carcinoma by serial dynamic contrast-enhanced MR imaging. Magn Reson Imaging 35:125–131
18. Chen FH, Wang CC, Liu HL et al (2016) Decline of tumor vascular function as assessed by dynamic contrast-enhanced magnetic resonance imaging is associated with poor responses to radiation therapy and chemotherapy. Int J Radiat Oncol Biol Phys 95:1495–1503

19. Rischke HC, Schafer AO, Nestle U et al (2012) Detection of local recurrent prostate cancer after radical prostatectomy in terms of salvage radiotherapy using dynamic contrast enhanced-MRI without endorectal coil. Radiat Oncol 7:185

20. Jost G, Endrikat J, Pietsch H (2017) The impact of injector-based contrast agent administration on bolus shape and magnetic resonance angiography image quality. Magn Reson Insights. https://doi.org/10.1177/1178623X17705894

21. Arlington Medical Resources (2014) The imaging market guide 2014 (German Edition).

22. Arlington Medical Resources (2014) The imaging market guide.

23. Weis M, Sommer V, Zollner FG et al (2016) Region of interest-based versus whole-lung segmentation-based approach for MR lung perfusion quantification in 2-year-old children after congenital diaphragmatic hernia repair. Eur Radiol 26:4231–4238

24. Weidner M, Zollner FG, Hagelstein C et al (2014) High temporal versus high spatial resolution in MR quantitative pulmonary perfusion imaging of two-year old children after congenital diaphragmatic hernia repair. Eur Radiol 24:2427–2434

25. Bhargava R, Hahn G, Hirsch W et al (2013) Contrast-enhanced magnetic resonance imaging in pediatric patients: review and recommendations for current practice. Magn Reson Insights 6:95–111

26. Boos M, Lentschig M, Scheffler K, Bongartz GM, Steinbrich W (1998) Contrast-enhanced magnetic resonance angiography of peripheral vessels. Different contrast agent applications and sequence strategies: a review. Invest Radiol 33:538–546

27. Essig M, Shiroishi MS, Nguyen TB et al (2013) Perfusion MRI: the five most frequently asked technical questions. AJR Am J Roentgenol 200:24–34

28. Zollner FG, Daab M, Sourbron SP, Schad LR, Schoenberg SO, Weisser G (2016) An open source software for analysis of dynamic contrast enhanced magnetic resonance images: UMMPerfusion revisited. BMC Med Imaging 16:7

29. Zollner FG, Weisser G, Reich M et al (2013) UMMPerfusion: an open source software tool towards quantitative MRI perfusion analysis in clinical routine. J Digit Imaging 26:344–352

30. Ostergaard L, Weisskoff RM, Chesler DA, Gyldensted C, Rosen BR (1996) High resolution measurement of cerebral blood flow using intravascular tracer bolus passages. Part I: Mathematical approach and statistical analysis. Magn Reson Med 36:715–725

31. Sourbron SP, Buckley DL (2013) Classic models for dynamic contrast-enhanced MRI. NMR Biomed 26:1004–1027

32. Watanabe Y, Dohke M, Okumura A et al (2000) Dynamic subtraction contrast-enhanced MR angiography: technique, clinical applications, and pitfalls. Radiographics 20:135–152 discussion 152–153

33. Kopka L, Vosshenrich R, Rodenwaldt J, Grabbe E (1998) Differences in injection rates on contrast-enhanced breath-hold three-dimensional MR angiography. AJR Am J Roentgenol 170:345–348

34. Zhang H, Maki JH, Prince MR (2007) 3D contrast-enhanced MR angiography. J Magn Reson Imaging 25:13–25

35. Wang J, Chen LT, Tsang YM, Liu TW, Shih TT (2004) Dynamic contrast-enhanced MRI analysis of perfusion changes in advanced hepatocellular carcinoma treated with an antiangiogenic agent: a preliminary study. AJR Am J Roentgenol 183:713–719

36. Thng CH, Koh TS, Collins DJ, Koh DM (2010) Perfusion magnetic resonance imaging of the liver. World J Gastroenterol 16:1598–1609

37. Choi SH, Lee JH, Choi YJ et al (2017) Detection of local tumor recurrence after definitive treatment of head and neck squamous cell carcinoma: histogram analysis of dynamic contrast-enhanced T1-weighted perfusion MRI. AJR Am J Roentgenol 208:42–47

38. Boll DT, Merkle EM, Lewin JS (2004) Low-flow vascular malformations: MR-guided percutaneous sclerotherapy in qualitative and quantitative assessment of therapy and outcome. Radiology 233:376–384

39. Krishnamurthy R, Bahouth SM, Muthupillai R (2016) 4D Contrast-enhanced MR angiography with the keyhole technique in children: technique and clinical applications. Radiographics 36:523–537

40. Wright KL, Seiberlich N, Jesberger JA et al (2013) Simultaneous magnetic resonance angiography and perfusion (MRAP) measurement: initial application in lower extremity skeletal muscle. J Magn Reson Imaging 38:1237–1244

41. Carroll TJ, Korosec FR, Swan JS, Hany TF, Grist TM, Mistretta CA (2001) The effect of injection rate on time-resolved contrast-enhanced peripheral MRA. J Magn Reson Imaging 14:401–410

42. Hartung MP, Grist TM, Francois CJ (2011) Magnetic resonance angiography: current status and future directions. J Cardiovasc Magn Reson 13:19

43. Wetzl J, Forman C, Wintersperger BJ et al (2017) High-resolution dynamic CE-MRA of the thorax enabled by iterative TWIST reconstruction. Magn Reson Med 77:833–840

44. Dietrich O, Raya JG, Reeder SB, Reiser MF, Schoenberg SO (2007) Measurement of signal-to-noise ratios in MR images: influence of multichannel coils, parallel imaging, and reconstruction filters. J Magn Reson Imaging 26:375–385

45. Hadizadeh DR, Jost G, Pietsch H et al (2014) Intraindividual quantitative and qualitative comparison of gadopentetate dimeglumine and gadobutrol in time-resolved contrast-enhanced 4-dimensional magnetic resonance angiography in minipigs. Invest Radiol 49:457–464

46. Ludemann L, Nafz B, Elsner F et al (2009) Absolute quantification of regional renal blood flow in swine by dynamic contrast-enhanced magnetic resonance imaging using a blood pool contrast agent. Invest Radiol 44:125–134

47. Ludemann L, Nafz B, Elsner F et al (2011) Dependence of renal blood flow on renal artery stenosis measured using CT angiography. Rofo 183:267–273

48. Warmuth C, Nagel S, Hegemann O, Wlodarczyk W, Ludemann L (2007) Accuracy of blood flow values determined by arterial spin labeling: a validation study in isolated porcine kidneys. J Magn Reson Imaging 26:353–358